Assessing the Conformational Changes of pb5, the Receptor-binding Protein of Phage T5, upon Binding to Its *Escherichia coli* Receptor FhuA*

Cécile Breyton[‡§¶1], **Ali Flayhan**[‡§¶2], **Frank Gabel**[‡§¶], **Mathilde Lethier**[‡§¶3], **Grégory Durand**[‖**], **Pascale Boulanger**[‡‡], **Mohamed Chami**[§§], **and Christine Ebel**[‡§¶]

*From the ‡Université Grenoble Alpes, Institut de Biologie Structurale (IBS), F-38027 Grenoble, France, §CNRS, UMR5075, IBS, F-38027 Grenoble, France, the ¶Commissariat à l'Energie Atomique, DSV, IBS, F-38027 Grenoble, France, the ‖Université d'Avignon, Equipe Chimie Bioorganique et Systèmes Amphiphiles, F-84029 Avignon, France, the **Institut des Biomolécules Max Mousseron, UMR 5247, F-34093 Montpellier, France, the ‡‡Institut de Biochimie et de Biophysique Moléculaire et Cellulaire, Université Paris-Sud, UMR CNRS 8619, F-91405 Orsay, France, and the §§Center for Cellular Imaging and NanoAnalytics, Biozentrum, University Basel, CH-4058 Basel, Switzerland*

Background: Little is known about the very first steps of infection of bacterial viruses.
Results: We specifically access the structure of phage T5 receptor-binding protein bound to its membrane receptor using specific techniques in small angle neutron scattering.
Conclusion: There are no large conformational changes.
Significance: Signal transduction within T5 appears different from that of phages binding cell wall saccharides.

Within tailed bacteriophages, interaction of the receptor-binding protein (RBP) with the target cell triggers viral DNA ejection into the host cytoplasm. In the case of phage T5, the RBP pb5 and the receptor FhuA, an outer membrane protein of *Escherichia coli*, have been identified. Here, we use small angle neutron scattering and electron microscopy to investigate the FhuA-pb5 complex. Specific deuteration of one of the partners allows the complete masking in small angle neutron scattering of the surfactant and unlabeled proteins when the complex is solubilized in the fluorinated surfactant F_6-DigluM. Thus, individual structures within a membrane protein complex can be described. The solution structure of FhuA agrees with its crystal structure; that of pb5 shows an elongated shape. Neither displays significant conformational changes upon interaction. The mechanism of signal transduction within phage T5 thus appears different from that of phages binding cell wall saccharides, for which structural information is available.

Bacteriophages are the most abundant microorganisms in the biosphere. At the origin of major discoveries in modern genetics, their study is gaining increasing popularity in fields as diverse as ecology, genetics, phylogeny, and nanophysics (1, 2). Phagotherapy is also blooming with the increased multiresistance of human, animal, and plant pathogens to antibiotics (3,

4). Furthermore, deciphering the sophisticated but minimalist phage molecular machineries elaborated for host cell recognition and infection is fascinating. Structural data have revealed horizontal gene transfer, masked at the sequence level by rapid evolution, from phages to bacteria, of machineries developed for bacterial pathogenicity (*e.g.* Type VI secretion systems, reviewed in Ref. 5).

The vast majority of bacteriophages, *Caudovirales*, are tailed phages that have an icosahedral protein capsid containing a densely packed double-stranded DNA and a tail with an adsorption device at its end that serves to recognize the cell surface and deliver the phage genome into the bacterium cytoplasm. In the case of lytic phages, the biosynthetic host machinery is then hijacked to transcribe the viral genome and produce new virions. The interaction between the phage receptor-binding protein (RBP)[4] and its bacterial receptor is the key signal that leads to capsid opening and cell wall perforation, resulting in the ejection of the DNA from the capsid into the cytoplasm, across the complex host envelope. Our aim is to describe the conformational rearrangements that initially take place between the RBP and its receptor. The coliphage T5 is an excellent model to study phage-host interactions for the following reasons: (i) both its RBP, pb5 (6), and its receptor, the *E. coli* outer membrane iron-ferrichrome transporter FhuA, have been identified and purified; (ii) the mere interaction between T5 and FhuA, either detergent-solubilized or reconstituted in liposomes, is enough to induce DNA ejection (7); and (iii) the interaction between purified pb5 and FhuA yields a highly stable, stoichiometric complex (8). Furthermore, this complex is

---

[1] To whom correspondence should be addressed: Institute for Structural Biology, 41 Rue Jules Horowitz, F-38027 Grenoble Cedex 01, France. Tel.: 334-3878-3037; Fax: 334-3878-5494; E-mail: Cecile.Breyton@ibs.fr.
[2] Present address: Institute of Biology and Chemistry of Proteins, F-69 367 Lyon, France.
[3] Present address: European Molecular Biology Laboratory, Grenoble Outstation, F-38042, France.

[4] The abbreviations used are: RBP, receptor-binding protein; SANS, small angle neutron scattering; AUC, analytical ultracentrifugation; CMP, contrast match point; LDAO, *N,N*-dimethyldodecylamine *N*-oxide; R_g, radius of gyration; SEC, size exclusion chromatography; *h*FhuA and *h*pb5, hydrogenated FhuA and pb5, respectively; *d*FhuA and *d*pb5, deuterated FhuA and pb5, respectively.

Conformational Changes of pb5 upon Binding to FhuA

currently the only complex biochemically available between an outer membrane receptor and a phage RBP. FhuA is composed of a 22-β-strand barrel, which is obstructed by a globular domain, or the "plug." Large extracellular loops and loops of the plug form the ligand binding sites (9). pb5 appears to fold as a unique domain, which undergoes secondary structural changes and most probably a rigidification of its structure upon binding to FhuA (10). In parallel to crystallization attempts of the FhuA-pb5 complex, small angle neutron scattering (SANS) and electron microscopy (EM) have been chosen to investigate the conformational changes that occur in pb5 following FhuA binding.

SANS combined with contrast variation and specific deuterium labeling of proteins is a particularly powerful technique to monitor conformational changes undergone by each protein within a complex. The neutron scattering length of the hydrogen nucleus is negative, whereas that of deuterium (and of most of the atoms) is positive. The difference between the scattering of the macromolecule and that of the solvent is proportional to a *contrast term* that can be modulated by changing the hydrogen content of the macromolecule or of the solvent by deuterium labeling. Very importantly, the contrast term of proteins vanishes in a buffer containing an appropriate H_2O/D_2O mixture at the contrast match point (CMP), expressed in D_2O %. Thus, the signal of a partner within a protein complex can be selectively highlighted or suppressed (11–13).

Purified membrane protein samples comprise at least one additional component, detergent, present as bound detergent and as free micelles. Thus, detergents need to be either matched or modeled, in order to obtain structural information from the non-matched protein partner. Fluorinated surfactants share with detergents their amphipathic structure (Scheme 1). They have been investigated as potential mild surfactants (14–18). F_6-Diglu (19, 20) and the chemically related and easier to synthesize F_6-DigluM (21) (Scheme 1A) are stabilizing toward membrane proteins and form homogeneous and globular micelles and well defined membrane protein complexes. The CMPs of F_6-Diglu (20) and of F_6-DigluM (11) are close to that of most proteins (20), making these fluorinated surfactants ideal candidates for SANS study of solubilized membrane protein complexes; both hydrogenated protein partner(s) and surfactant will be matched simultaneously, allowing us to focus on deuterated protein partner(s) only.

Here, we have analyzed the FhuA-pb5 complex solubilized in F_6-DigluM by SANS. A contrast matching strategy shown in Scheme 1B was defined to separately resolve each partner alone and within the complex. Hydrogenated proteins and the F_6-DigluM micelles were expected to both be contrast-matched at the same D_2O %, the observed signal being due to the deuterated partner protein. FhuA low resolution structure in solution, determined by SANS, is in very good agreement with its crystal structure. It remains unchanged upon formation of the complex. pb5 is shown to be an elongated protein, whose structure, at the resolution of the technique, does not show significant conformational changes upon binding to FhuA. The SANS envelopes of the complex and the individual proteins are in excellent agreement with negative stain single particle EM. We propose that the mechanism of signal transduction from the RBP to the rest of the phage within phage T5, and thus other
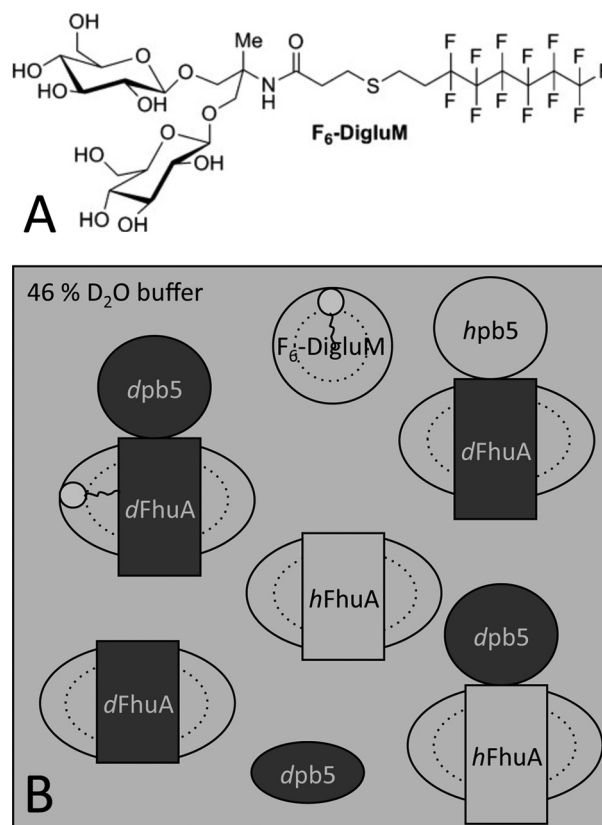
SCHEME 1. **SANS contrast strategy.** *A*, F_6-DigluM chemical structure; *B*, SANS contrast strategy to highlight specific parts of the protein-detergent complexes. Partially deuterated proteins are represented in *dark gray*. Hydrogenated proteins and the F_6-DigluM micelles are represented in *light gray* as is the 46% D_2O buffer in which they are contrast-matched.

siphophages with straight fibers binding protein receptors, is different from that of siphophages binding cell wall saccharides, for which structural information is available.

EXPERIMENTAL PROCEDURES

Chemicals

F_6-DigluM was synthesized by our general procedure consisting of one-pot reduction/alkylation of a thiol-based fluorinated chain onto an acrylamido-type polar head (19) with slight modifications. The 1H,1H,2H,2H-perfluorooctanethiol was directly used instead of its corresponding thioacetate (21), allowing the preparation of F_6-Diglu M in only three steps. F_6DigluM was purified by flash chromatography on silica gel (AcOEt/MeOH/H_2O, 7:2:1, v/v/v), followed by size exclusion chromatography on Sephadex LH 20 (MeOH). The solvent was removed under vacuum; the resulting powder was solubilized in MilliQ water and freeze-dried to give F_6DigluM as a white foam. 300 mg of F_6-DigluM was used in this study.

Adaptation, Overexpression, and Purification of d*FhuA* and h*FhuA* and of h*pb5* and d*pb5*

FhuA was purified from the *E. coli* strain AW740 transformed with a plasmid encoding the *fhuA* gene in which a His tag has been inserted in the extracellular loop L5 (22). pb5 was purified from the *E. coli* strain BL21(DE3) carrying the *oad* gene encoding pb5 fused to an N terminus His tag in a pET-28 vector

(8). Cells were grown in LB medium at 37 °C in the presence of 100 μM of the iron-chelating agent dipyridine for AW740 cells, and at 20 °C without induction for BL21(DE3) cells. To produce deuterated proteins, the two strains were first adapted to hydrogenated Enfors minimal medium for 7 days at 37 °C. Strains were then adapted to Enfors minimal medium in 80% D_2O for 5 days. AW740 cells were then grown for 48 h at 37 °C in the presence of 100 μM dipyridine. BL21(DE3) cells were grown at 20 °C, and overexpression of $d$pb5 was induced at $A_{600\,nm} = 0.9$ with 0.5 mM isopropyl 1-thio-β-D-galactopyranoside for 24 h. hFhuA, $d$pb5, and $h$pb5 purifications were carried out as described (10). For hFhuA, a molecular sieve step was added (SD200 10/300 GL; GE Healthcare; buffer: 20 mM Tris-HCl, pH 8.0, 150 mM NaCl, 0.05% *N,N*-dimethyldodecylamine *N*-oxide (LDAO)). dFhuA purification was performed as for hFhuA except that the anion exchange chromatography was omitted, because the deuterated protein remained adsorbed onto the matrix in the presence of 1 M NaCl. $d$pb5 and $h$pb5 were eluted from the cation exchange column (HTSP, 1 ml; GE Healthcare) in H_2O or 46% D_2O buffer and were used for data collection or complexation with FhuA.

Mass Spectrometry

LC/electrospray ionization-TOF-MS analysis was carried out on FhuA. The mass of hFhuA agrees with the sequence (79,965 *versus* 79,960 Da). The mass for dFhuA (82,930 Da) combined with the calculated mass (with deuteration of non-exchangeable H only, 84,061 Da) gives an estimate of 72% deuteration.

Surfactant Exchange, Formation of the FhuA-pb5 Complexes, and Quality Control of the Samples

First Series—SD200 fractions containing hFhuA or dFhuA solubilized in 0.05% LDAO were pooled and concentrated, desalted onto a PG10 column (3 ml; Bio-Rad), and loaded onto a 2-ml nickel-nitrilotriacetic acid home packed column (Qiagen resin) equilibrated in 20 mM Tris-HCl, pH 8.0, 0.05% LDAO. The flow-through, containing some unbound FhuA, was reloaded onto the column (6 cycles). The column was then washed with 10 ml of the equilibration buffer, and surfactant exchange was performed by washing the column with 20 ml of 20 mM Tris-HCl, pH 8.0, 2 mM F_6-DigluM. The protein was eluted with 20 mM Tris-HCl, pH 8.0, 4 mM F_6-DigluM, and 200 mM imidazole. To avoid excess of one of the partners, different FhuA-pb5 ratios were screened on small volumes and analyzed on SDS gels before formation of the complex on a preparative scale. Except for pb5, all samples were concentrated by ultrafiltration (Centricon 50) and finally dialyzed overnight against 2× 100 ml of 150 mM NaCl, 20 mM Tris-HCl, pH 8.0, 0.7 mM F_6-DigluM, 46% D_2O. Final protein concentrations were as follows: hFhuA, 4.5 mg/ml; dFhuA, 4.6 mg/ml; dFhuA-$h$pb5, 4.9 mg/ml; hFhuA-$d$pb5, 2.1 mg/ml; dFhuA-$d$pb5, 3.2 mg/ml. $d$pb5 was studied in H_2O buffer at 0.5 mg/ml.

Second Series—dFhuA or hFhuA monomer fractions of gel filtration were concentrated by ultrafiltration (30,000 molecular weight cut-off; Millipore) to ~8 mg/ml. Samples were supplemented with 10 mM + 2 g/g F_6-DigluM/protein (total concentration, ~32 mM) and incubated for 30 min. BioBeads

(Bio-Rad) were then added (100 mg/ml), and the samples were incubated on a rotating wheel at room temperature for 1 h. BioBeads were removed, and the FhuA/LDAO/F_6-DigluM mixture was submitted to size exclusion chromatography (SEC) (SD200 10/300 GL; buffer: 150 mM NaCl, 20 mM Tris-HCl, pH 8.0, 0.7 mM F_6-DigluM, 46% D_2O). Fractions of the second half of the monomer peak (to avoid any dimer contamination) were pooled and supplemented with 2 mM F_6-DigluM and, for half of the samples, with stoichiometric amounts of $d$pb5 to form the complexes. dFhuA, hFhuA, hFhuA-$d$pb5, and dFhuA-$d$pb5 samples were concentrated by ultrafiltration (molecular weight cut-off 30,000 and 100,000 (Millipore) for FhuA and the complexes, respectively) before another SEC equilibrated in the same buffer. 320-μl fractions were collected, and the most concentrated fractions of the second half of the peak were supplemented with 2 mM F_6-DigluM and directly used for SANS measurements. Final protein concentrations were as follows: hFhuA, 0.9 mg/ml; dFhuA, 0.8 mg/ml; hFhuA-$d$pb5, 1.0 mg/ml; dFhuA-$d$pb5, 1.2 mg/ml. $d$pb5 was also studied in 46% D_2O at 0.4 mg/ml.

In the two series, surfactant exchange was controlled by thin layer chromatography (solvent chloroform/methanol/water, 65:35:5) stained by sulfuric acid and heating (300 °C). No residual LDAO was detected (detection limit <0.005%). To check for the homogeneity of the samples, AUC was performed on the SANS samples, sometimes after a 2-fold dilution in 150 mM NaCl, 20 mM Tris-HCl, pH 8.0, 46% D_2O, using a Beckman-XLI ultracentrifuge at 42,000 rpm and 20 °C, in 3-mm optical path two-channel centerpieces, and analyzed as described (*e.g.* see Refs. 23 and 24). SEC was also performed for the second series. 10-μl aliquots were loaded onto an analytical SD200 5/150 column (GE Healthcare) in 150 mM NaCl, 20 mM Tris-HCl, pH 8.0, 0.7 mM F_6-DigluM, 46% D_2O.

Small Angle X-ray Scattering Experiments

Small angle x-ray scattering experiments were conducted on the ID14-3 beamline at the European Synchrotron Radiation Facility (Grenoble, France). The data were recorded using a two-dimensional Pilatus detector, with a monochromatic x-ray beam ($\lambda = 0.931$ Å) and a sample to detector distance of 2430 mm. The concentration of pb5 was 0.48 mg/ml in 25 mM MES buffer, pH 6.0, and 330 mM NaCl. 96 acquisitions (1 s/acquisition) were recorded during 300 s using 100 μl of sample in a continuous flow for both the protein and the buffer. The spectra were corrected individually for the response of the detector and scaled with respect to the incident beam intensity and the absorption of the samples. The averaged spectrum of the buffer was subtracted from the corrected averaged spectrum of pb5. A solution of bovine serum albumin at 4.94 mg/ml was used as a reference for the calibration of the spectra.

SANS Experiments

All samples were measured in Hellma quartz cells 100QS with 1-mm optical path length at the SANS instrument D22 at the Institute Laue-Langevin (Grenoble, France). The sample temperature was kept at 20 °C (first series) and 5 °C (second series) during the exposure times. Scattering data from all samples were recorded at two instrumental detector/collimator

configurations, 2m/2m and 8m/8m, using a neutron wavelength of $\lambda = 6$ Å.

SANS Data Analysis

At each instrumental configuration, water, the H_2O/D_2O buffers, the empty beam, an empty quartz cell, and a boron sample (electronic background) were measured. Exposure times varied between 20 min (empty cell, boron) and 150 min ($d$pb5 in 46% D_2O) according to the sample and instrument setup. Transmissions were measured during 2–3 min for each sample. The raw data were reduced (detector efficiency, electronic background, angular averaging) using a standard Institute Laue-Langevin software package (25) and normalized by the scattering of water. When applicable, the corrected scattered intensities from the two different Q ranges were merged ($Q = (4\pi/\lambda)\sin\theta$ is the modulus of the scattering vector, with 2θ being the scattering angle), and in all cases, the respective buffer signals were subtracted. The radii of gyration (R_g) and the intensities scattered in the forward direction ($I(0)$) of all samples were extracted by the Guinier approximation, with $R_g Q \leq 1.3$, using the program Primus (26). The analysis of $I(0)$ in terms of molar mass is done according to Ref. 27, $I(0)/c = (k/N_A)\Sigma M(\partial\rho_N/\partial c)^2$, where c represents the macromolecule weight concentration (g/liter), k is a geometrical factor, N_A is Avogadro's number, Σ is for the different types of macromolecule in solution, and M and $\partial\rho_N/\partial c$ are their molecular mass and neutron scattering length density increment (cm/g). For a homogeneous macromolecule, $\partial\rho_N/\partial c = \Sigma b/M - \rho_N°\bar{v}$, where Σb is the sum of the scattering lengths of the constituting atoms, $\bar{v}$ is the partial specific volume (cm³/g) of the macromolecule, and $\rho_N°$ is the solvent neutron scattering length density (cm^{-2}). For a multicomponent complex comprising deuterated and hydrogenated macromolecules, we use the derived equation, $I(0)/c_d = (k/N_A)M_d(\partial\rho_N/\partial c_d)^2$, where c_d is the concentration of the deuterated partner; $\partial\rho_N/\partial c_d = (\partial\rho_N/\partial c)_d + M_h/M_d(\partial\rho_N/\partial c)_h$, the second contribution being null at 46% D_2O. Numerical values are in Ref. 11.

Low Resolution Models Determined by ab initio Analysis

We used the program DAMMIF (28) to generate low resolution envelopes of FhuA, of pb5 alone or within the complex, and of the complex from the SANS data, and of pb5 from the small angle x-ray scattering data. We used several variations of the input parameters in the default mode to model the data. Data up to $Q_{max} = 0.15$–0.2 Å^{-1} were included. The DAMMIF input files were generated using the program GNOM (29), imposing the restraints $p(r = 0) = 0$ and $p(r = D_{max}) = 0$ for the pair distance distribution function $p(r)$. For each sample, the values of D_{max} were varied to obtain the best fit of the data and a smooth $p(r)$ curve. As a quality control, the radii of gyration determined from the pair distribution analyses were compared with the ones determined by the Guinier analysis. 10–30 DAMMIF models were averaged using DAMAVER (30). The experimental curve for the dFhuA data was compared with the Protein Data Bank structure 2FCP of FhuA using CRYSON (31), applying a 72% deuteration degree of the protein, as determined by mass spectrometry.

Transmission Electron Microscopy and Image Processing

Samples were diluted at 0.01 mg/ml in 20 mM Tris-HCl, pH 8.0, 150 mM NaCl, 0.05% LDAO. Aliquots of 5 μl were adsorbed onto a glow-discharged carbon film-coated copper grid, washed with three droplets of pure water, and subsequently stained with 2% uranyl-acetate. Images were recorded using a Philips CM10 microscope operating at 80 kV on a Veleta 2000 × 2000 CCD camera (Olympus).

Reference-free alignment was performed on manually selected particles from digitized electron micrographs using the EMAN image processing package (32). After using a reference-free alignment procedure, particle projections were classified by multivariant statistical analysis. The class averages with the best signal/noise ratio were selected and gathered in a gallery.

RESULTS

F_6-DigluM in SANS Can Be Matched Homogeneously in the Whole Q Range—F_6-DigluM scattering was measured at 10.0 mg/ml in H_2O and at 3.2, 6.4, and 9.7 mg/ml in 100% D_2O. It displays a very neat, linear Guinier plot (Fig. 1*A*), indicative of well defined globular particles. The derived radii of gyration (R_g) are 1.87 ± 0.02 nm (H_2O) and 2.05 ± 0.01 nm (D_2O). An estimate of the critical micellar concentration (0.7 mM) in D_2O can be obtained from the change of the forward scattering intensity $I(0)$ with the total concentration, c, of surfactant. This value is close to the value determined from tensiometry and analytical ultracentrifugation (AUC) measurements (0.38 and 0.48 mM, respectively) (21). From an absolute calibration of $I(0)$, a molecular mass of 64 ± 2 kDa can be calculated in D_2O for F_6-DigluM micelles, close to the value of 47 kDa from AUC, considering a globular shape, the difference being most probably related to the inaccuracy of the partial specific volume. A match point of 46% D_2O is derived from the $\sqrt{(I(0)/(c - cmc)T)}$ plot, with cmc the critical micellar concentration and T the sample transmission, close to the calculated one of 49% (11). The R_g, critical micellar concentration, molar mass, and match point are close to those measured by SANS for the very similar F_6-Diglu (20). Neutron scattering was measured for F_6-DigluM at 17.6 mg/ml (20 mM) in 150 mM NaCl, 20 mM Tris-HCl, pH 8.0, 46% D_2O. Fig. 1*B* shows that the scattering of F_6-DigluM is indistinguishable from that of the solvent. Thus, F_6-DigluM not only is globally matched at the forward direction ($Q = 0$) but also displays no structural features in the investigated Q range. This is not common for surfactants, for which hydrophobic tail and hydrophilic head do not have the same chemical composition (11). The match point of F_6-DigluM, as for F_6-Diglu, corresponds roughly to that of hydrogenated proteins, which is highly interesting for SANS studies of membrane protein complexes in combination with specific deuteration.

Production and Quality Control of the SANS Samples—In view of our strategy (Scheme 1*B*), pb5 and FhuA were individually overproduced and purified, according to published protocols for the hydrogenated protein. Deuterated proteins were purified from *E. coli* stains adapted to 80% D_2O in minimal medium, with slight modifications in the purification (see "Experimental Procedures"), leading to the purification of 1.5 mg of $d$pb5 and 2 mg of dFhuA per liter of culture. The deu-
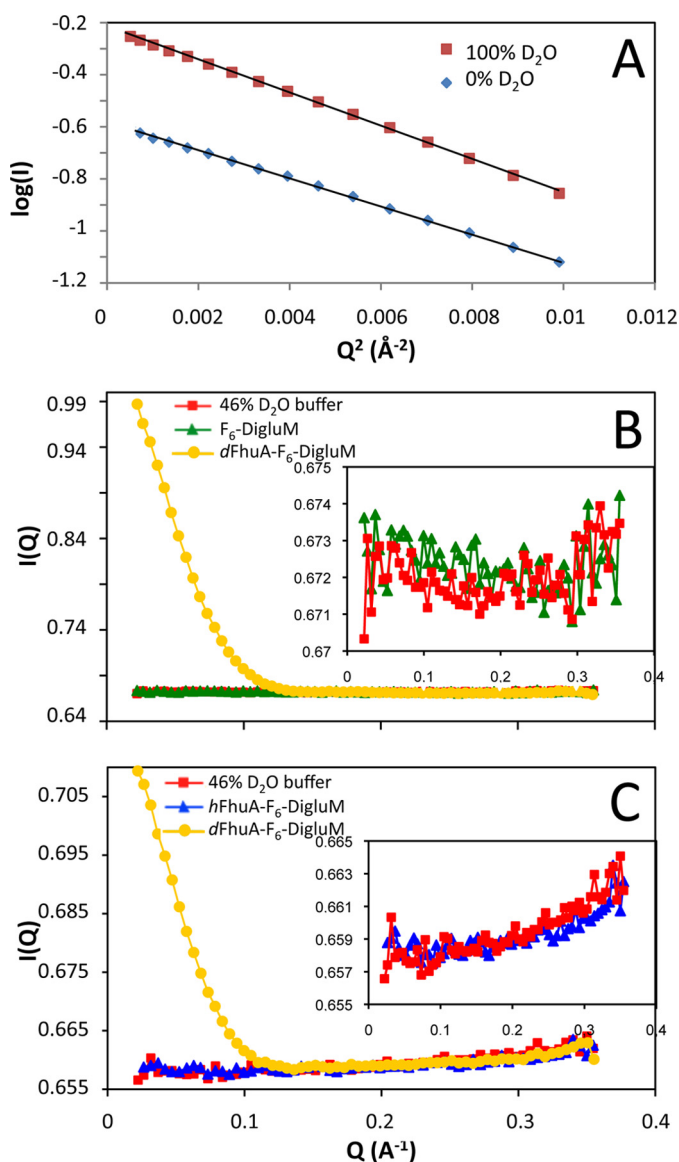
FIGURE 1. **SANS of F$_6$-DigluM and validation of SANS strategy.** *A*, Guinier plot of F$_6$-DigluM (10 mg/ml) in 0% (*triangles*) or 100% D$_2$O (*squares*). *B* and *C*, scattering curves, before buffer subtraction, of F$_6$-DigluM (17.6 mg/ml; *B, triangles*) and *h*FhuA (4.5 mg/ml; *C, triangles*) in F$_6$-DigluM (8 mg/ml free micelles from AUC), measured in 46% D$_2$O buffer, compared with the scattering curve of the 46% D$_2$O buffer (*squares* in *B* and *C*) and *d*FhuA in F$_6$-DigluM (*circles* in *B* and *C*). *d*FhuA was at 4.6 (*B*) and 0.8 (*C*) mg/ml, and AUC estimated 9 (*B*) and 2.3 (*C*) mg/ml free micelles. *Insets*, enlargements of the buffer curves.

teration rate, estimated for *d*FhuA using mass spectrometry, was ~72%.

Two series of SANS experiments were performed with surfactant and solvent exchange following two different protocols: (i) affinity chromatography, mixture of the partners, dialysis, and concentration, and (ii) incubation with BioBeads, SEC, concentration, mixture of the partners, and SEC. These protocols led to sample concentrations of 2–4 and ~1 mg/ml, respectively. In the first protocol, some of the samples contained aggregates, detected by SANS and AUC, and satisfactory samples were found only for *h*FhuA, *d*FhuA, and *d*FhuA-*h*pb5. The second protocol, avoiding final concentration steps, was thus designed to fulfill the requirements of full surfactant exchange, taking into account the limited availability of F$_6$-
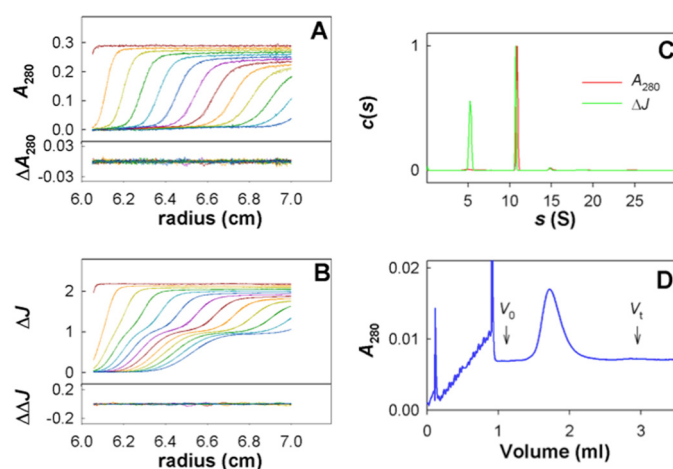

FIGURE 2. **AUC and SEC quality control for *d*FhuA and *d*FhuA-*d*pb5 sample following SANS.** *A* and *B*, superposition of experimental and fitted sedimentation velocity profiles obtained in 3-mm optical path length cells during 2 h at 42,000 rpm at 20 °C (*top subpanels*) and their differences (*bottom subpanels*), at 284 nm (*A*) and using interference optics (*B*), for *d*FhuA SANS sample in 46% D$_2$O (second protocol) after 4-day storage at 4 °C. *C*, Sedimentation coefficient distributions *c*(*s*). The distributions are normalized to the main protein peak value. *D*, SEC of the *d*FhuA-*d*pb5 SANS sample (second protocol), loaded after the SANS measurements onto an SD200 5/150 column in 20 mM Tris-HCl, pH 8, 150 mM NaCl, 0.7 mM F$_6$-DigluM, 46% D$_2$O, run at 0.45 ml/min. Void volume (*V$_0$*) = 1.12 ml; total volume (*V$_t$*) = 2.83 ml.

DigluM, control of the D$_2$O content, and sample homogeneity, with protein concentrations compatible with SANS analysis. Sample homogeneity was checked after SANS experiments by AUC and analytical SEC. Fig. 2 shows sedimentation velocity AUC analysis for *d*FhuA. F$_6$-DigluM micelles are detected mainly using the interference optics at 5.3 ± 0.2 S, at a concentration, from fringe shifts, of ~3 mM (for the second protocol) in the SANS samples. The main species is detected at 10.7 S for *d*FhuA. Similar results were obtained for *h*FhuA, *h*FhuA-*d*pb5, *d*FhuA-*h*pb5, and *d*FhuA-*d*pb5, with main peaks obtained at 10.4, 11.5, 11.8, and 11.9 ± 0.2 S, the variation in the *s* values being logically related to the deuteration level, deuterated molecules being more dense than hydrogenated ones. The combined analysis of the absorbance and interference signals gave an identical amount, in mol/mol, of bound F$_6$-DigluM of 130 ± 15 and 130 ± 45 for FhuA and FhuA-pb5, respectively. The derived frictional ratio of 1.28 for *d*FhuA and 1.35 for the complexes considered as monomer are close to that of 1.25 expected for a globular compact shape. Larger species were also detected in limited amounts (~5%) in both protocols, the second one, however, leading to more homogeneous samples. In the case of the complexes, aggregates are detected in AUC in larger amounts, a feature probably related to pb5 sensitivity to pressure and propensity to aggregate at a concentration above 0.5 mg/ml, because they were undetected in SEC (Fig. 2*D*) and in the SANS analysis.

Hydrogenated Proteins Are Masked in SANS at the CMP of F$_6$-DigluM—Because the CMP of F$_6$-DigluM is close to that of most proteins (~44% D$_2$O), it is expected that both surfactant and hydrogenated proteins can be matched in the same buffer condition. Fig. 1*C* shows the scattering curve of *h*FhuA solubilized in F$_6$-DigluM at 46% D$_2$O. It clearly shows that *both* *h*FhuA and F$_6$-DigluM are indeed indistinguishable from the
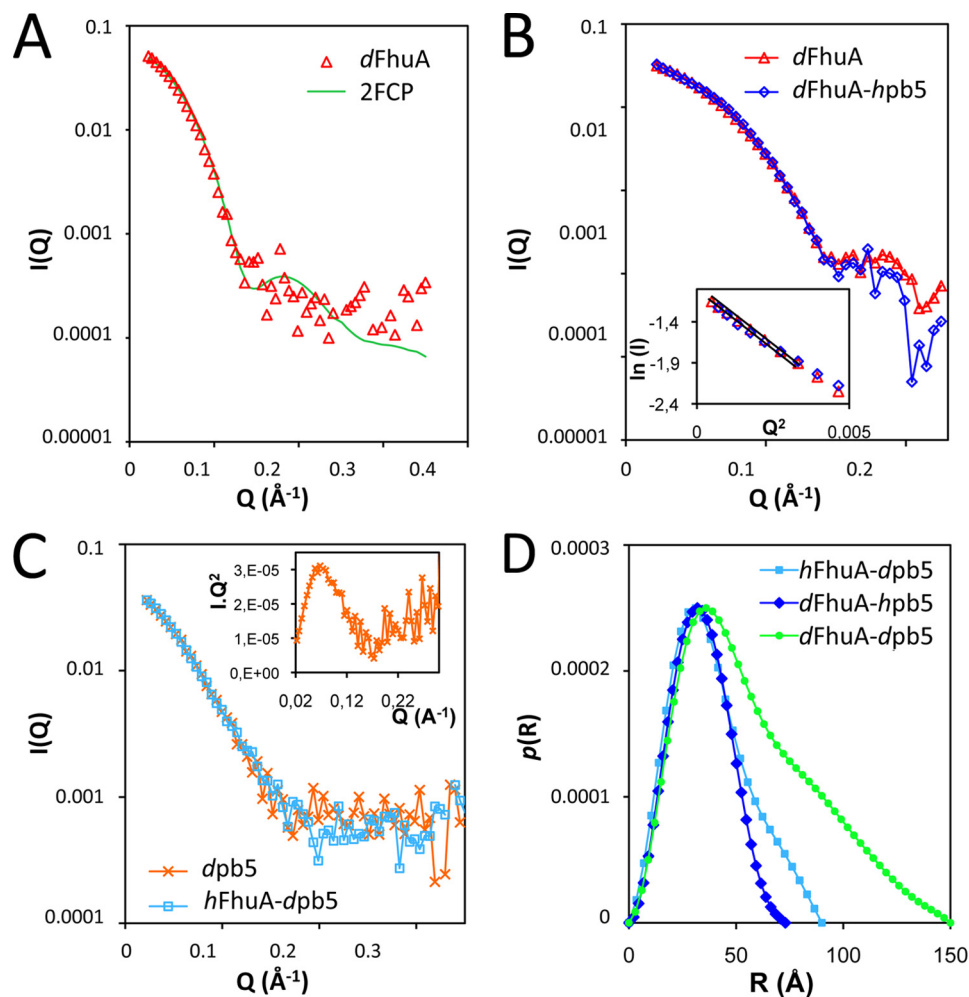
FIGURE 3. **SANS analysis of FhuA, pb5, and complex.** *A*, calculated and measured scattering curve of *d*FhuA solubilized in F_6-DigluM (*triangles*) at 46% D_2O. The 2FCP curve was calculated with the program Cryson, considering a 46% D_2O buffer and a 72% deuterated protein (*solid line*). $\chi^2 = 1.173$ on the whole Q range. *B*, experimental scattering curves of isolated *d*FhuA solubilized in F_6-DigluM (*triangles*) or in complex with *h*pb5 (*diamonds*). *Inset*, Guinier analysis of the two data sets. *C*, scattering curves of *d*pb5 alone (crosses) or in complex with *h*FhuA solubilized in F_6-DigluM (*squares*) measured in 46% D_2O. *Inset*, Kratky representation of the *d*pb5 sample. *D*, pair distance distribution function, *p*(*r*), calculated using Gnom, of *h*FhuA-*d*pb5 (*squares*), *d*FhuA-*h*pb5 (*diamonds*), and *d*FhuA-*d*pb5 (*circles*) samples measured in a 46% D_2O buffer.

buffer, showing no structural feature in the investigated Q range.

The Low Resolution SANS Structures of FhuA Alone and in Complex with pb5 Are Identical to the Crystal Structure—Fig. 3*A* shows the scattering curve of isolated *d*FhuA, solubilized in F_6-DigluM, at 46% D_2O. The measured data fit perfectly well with the calculated scattering curve of FhuA (Protein Data Bank entry 2FCP).

In order to detect conformational changes induced upon formation of a complex with pb5, scattering data of *d*FhuA solubilized in F_6-DigluM in complex with *h*pb5 were recorded. As shown in Fig. 3*B*, the data are superimposable, suggesting that the FhuA structure remains unchanged upon binding of pb5. The Guinier analyses of the two data sets (Fig. 3*B*, *inset*) allow the extrapolation of the forward intensities, which, normalized by FhuA concentration, are insignificantly different for *d*FhuA and for *d*FhuA-*h*pb5 samples, and correspond to FhuA as a monomer with 85% deuteration. The derived R_g are 28.1 ± 0.3 and 27.8 ± 0.2 Å for *d*FhuA and for *d*FhuA-*h*pb5, respectively. Both results corroborate the complete masking of *h*pb5

and the absence of conformational changes in the structure of FhuA upon formation of the complex. As expected from the nice superpositions of the curves, *ab initio* modeling of the *d*FhuA and *d*FhuA-*h*pb5 at 46% D_2O shows very similar cylindrical volumes, ~75 Å long and ~50 Å wide, in which the Protein Data Bank structure of FhuA fits very well (Fig. 4*A*).

SANS Structure of pb5 Alone and in Complex with FhuA— pb5 has a strong tendency to aggregate whenever concentrated or dialyzed or at concentrations above 0.5 mg/ml. Thus, sample preparation had to be optimized without protein concentration, and the most concentrated fraction of the cation exchange chromatography was recovered and immediately diluted to 0.5 mg/ml if exceeding this concentration. However, even at these relatively low concentrations, interpretable SANS data of the *d*pb5 samples could be recorded (Fig. 3*C*), in particular for *d*pb5 in H_2O buffer, where contrast is maximal. A Kratky representation of the data displays a bell shape, suggesting that pb5 is a compact protein, showing no sign of unfolding or structural disorder (Fig. 3*C*, *inset*) (33). Neutron diffraction curves of *d*pb5 measured either in 46% D_2O or in H_2O or x-ray diffusion curves
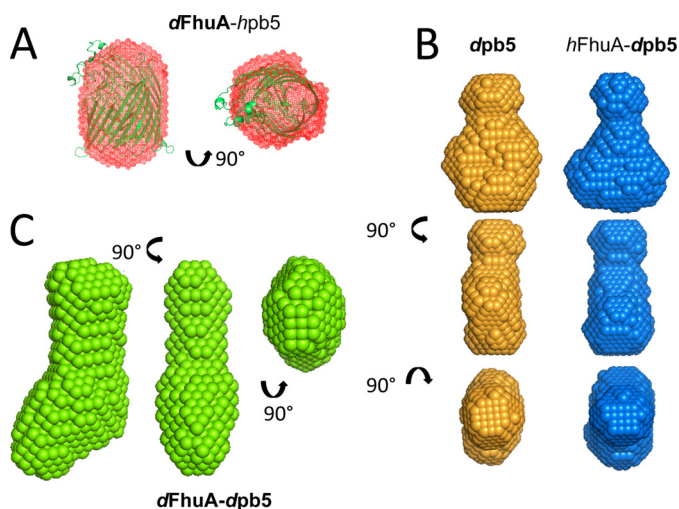
FIGURE 4. **Ab initio envelopes from SANS.** *Ab initio* envelopes (at 46% D$_2$O) of *d*FhuA-*h*pb5 (*red mesh*), superimposed with the crystal structure of FhuA (2FCP, *green*) (*A*); *d*pb5 (*orange*) and *h*FhuA-*d*pb5 (*blue*) (*B*); and *d*FhuA-*d*pb5 (*C*). 10 (*d*FhuA-*h*pb5) and 20 (*d*pb5, *h*FhuA-*d*pb5, and *d*FhuA-*d*pb5) independent, very similar structures, calculated using Dammif, were averaged using DAMAVER. *Side* and *top views* are shown.

FIGURE 5. **Negative stain electron microscopy.** *A*, negative stain electron microscopy of purified FhuA (*left*), pb5 (*middle*), and FhuA-pb5 complex (*right*). The *insets* are their corresponding averages of the major classes. *Scale bar*, 50 nm; *inset base line*, 20 nm. *B*, FhuA and pb5 proteins are identified on the FhuA-pb5 complex.

of pb5 were superimposable, modulo the hydration shell, and so were their derived pair distance distribution functions (not shown). *Ab initio* modeling reveals an elongated, scamorza-shaped molecule (Fig. 4*B*), with a maximum distance of 90 Å and a width of ~20–60 Å. Fig. 3*C* shows the scattering curve of *d*pb5, alone or in complex with *h*FhuA, both in a 46% D$_2$O buffer, where *h*FhuA and F$_6$-DigluM are masked. The two curves, like their derived pair distribution functions (not shown), are very similar, indicating that pb5 does not undergo important conformational changes upon binding of FhuA. Radii of gyration of 28.0 ± 1.2 and 29.6 ± 0.9 Å were extracted for *d*pb5 and *h*FhuA-*d*pb5, respectively, suggesting a slight elongation of pb5 within the complex. However, it cannot be excluded that this small difference is due to residual contributions from the *h*FhuA-F$_6$DigluM moiety of the complex.

SANS Structure of the Complex—The overall structure of the complex can be obtained by measuring SANS data on a *d*pb5-*d*FhuA complex solubilized in F$_6$-DigluM in a 46% D$_2$O buffer. A molar mass of 196 ± 41 Da (*i.e.* compatible with a 1:1 complex of 151 kDa) and an R_g of 49.2 ± 0.9 Å are extracted from the Guinier plot, and GNOM allows determination of D_{max} = 150 Å (Fig. 3*D*). *Ab initio* modeling reveals an elongated particle, with a socklike shape (Fig. 4*C*). The shape and dimensions of the *d*FhuA-*d*pb5 complex are compatible with a longitudinal organization of the individual FhuA and pb5 proteins. Without further constraints in the SANS data, the resolution (~30 Å) is, however, too low to allow fitting of the individual proteins within the envelope.

EM Negative Stain Data Structure of the FhuA-pb5 Complex—FhuA, pb5, and the complex were analyzed by EM and single particle analysis of negatively stained sample, the particles being too small to be visualized by cryo-EM. Fig. 5 shows the overall projection structure of FhuA, pb5, and the complex. The dimensions of FhuA are in agreement with the crystal structure (height of 70 Å). pb5 protein has an elongated shape, 80 Å long and 50 Å wide, and presents a slightly sharp extremity. There is
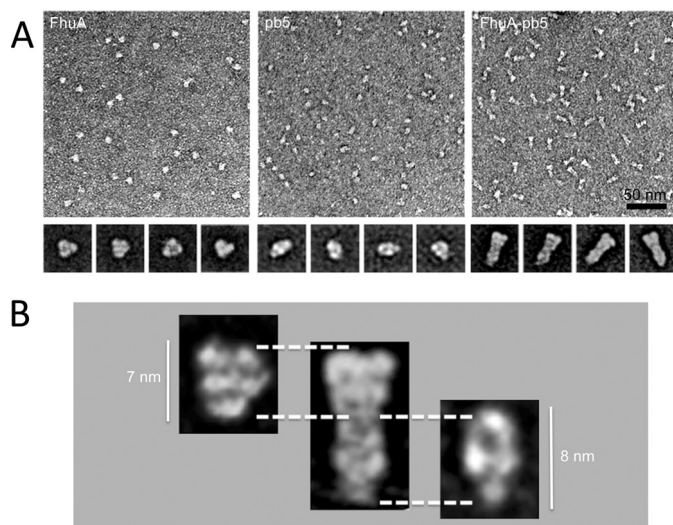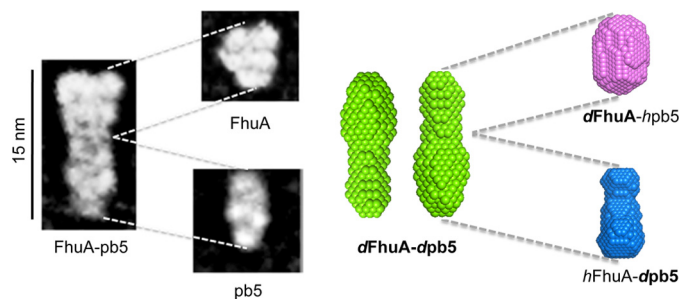

FIGURE 6. **Comparison of the EM and SANS projections.** *Left*, EM; *right*, SANS. The overall dimensions of the SANS and EM molecules coincide. Two SANS projections are presented, rotated by 180° because the relative position of FhuA and pb5 is not determined by the resolution. Projections are drawn to scale.

a good agreement between pb5 structures determined by SANS and by EM (Fig. 6). The dimensions and overall shape of the complex are also similar between SANS and EM data, with an elongated shape of 150 Å long, even if the reconstituted volumes do not perfectly coincide. The slight differences may be attributed to the differences in the techniques (see "Discussion"). The localization of each protein within the EM complex projection is facilitated by the substructures within each protein (Fig. 5*B*). The peaked side of pb5 is recognizable at the extremity of the complex. Even if the different partners within the complex are not distinguished individually, the EM data strongly suggest that, at this resolution and in agreement with SANS data, there are no noticeable conformational changes of pb5 upon complex formation.

DISCUSSION

In this study, we validate the use of F$_6$-DigluM for low resolution studies of individual protein partners within a membrane protein complex using SANS. Conformational changes, if occurring, can be monitored. For all practical purposes, F$_6$-DigluM (34) can be considered as homogeneous, matched on the whole *Q* range. Therefore, sophisticated modeling of deter-

gent residuals and very careful control of detergent concentration in the sample can be avoided. Usually, hydrophobic tails and hydrophilic heads have different CMPs (due to their different chemical composition) and will contribute to the scattered signal (see Ref. 11 and references therein). Only a very limited number of other detergents, such as Foscholine12 (35), can be considered as homogeneously matched in practice. However, F_6-DigluM has the particular property of very similar scattering length densities, for both head and tail on the whole D_2O % range, similar to hydrogenated proteins (11). This allows specific investigation of a protein subunit, if deuterated, within a membrane protein complex. A similar achievement was obtained by combining partial protein deuteration and appropriate mixing of deuterated and hydrogenated SDS (36). The advantage of F_6-DigluM is that it can be used with a wide range of membrane proteins and that it is potentially less denaturating than most commonly used detergents (15). Importantly, in our study, F_6-DigluM provided samples of required homogeneity for SANS.

In this study, we have determined for the first time, using SANS and EM, the low resolution structure of the receptor-binding protein of a *Siphoviridae* infecting Gram-negative bacteria. From both techniques, pb5 appears to be elongated and compact with a maximum dimension of ~80–90 Å. This is in agreement with the limited proteolysis results suggesting that the protein folds as a unique and compact domain (10).

SANS, combined with the use of F_6-DigluM and specific deuteration of one of the partners, shows no large structural rearrangements of either partner upon formation of the complex (Figs. 3 and 4). Note that even at low resolution, rather minor conformational changes can be distinguished by small angle scattering. For example, in the two multidomain proteins, adenylate cyclase (23.5 kDa) and lactoferrin (78.2 kDa), a small domain (17 and 22% of the protein mass) undergoes ~60–70° rotation with respect to the rest of the protein upon ligand binding. These conformational changes are reflected by very distinguishable scattering curves (36). The absence of structural rearrangements in FhuA is consistent with its crystal structure alone or bound to different ligands showing only little, rigid body, conformational changes of extracellular loops (see Ref. 9 for a review). A dynamic behavior of the plug has recently been reported from destabilization by urea (37). However, our results definitely rule out the possibility of the plug domain of FhuA or part of it being removed from the barrel upon pb5 binding (*e.g.* to allow the DNA through the barrel of FhuA, a mechanism already eliminated from electron microscopy studies) (38). Concerning pb5, the invariance of its shape upon binding to FhuA from SANS and EM analysis was instead unexpected because binding information needs to be transmitted to the rest of the phage (see below).

The overall envelope and projection of the FhuA-pb5 complex determined by SANS and EM are similar (Fig. 6), even if the SANS envelope of the complex presents a slight curved shape that is not apparent in the EM projection. We should keep in mind, however, that both techniques sample different objects; the EM projections result from stained, possibly oriented and dried particles that are picked individually and averaged. We cannot rule out that staining induces slight distortions of the particle. SANS, on the other hand, is a mean of *all* particles present in the solution sample, including aggregates (if present) and averaging conformations in dynamic equilibrium. Significant differences in EM and small angle x-ray scattering envelopes were, for example, observed in subcomplexes of the type 6 secretion system (39). Furthermore, in the EM structure of our membrane complex, the detergent could contribute to the signal, whereas it does not for the SANS data. Thus, the two envelopes do not represent exactly the same object. However, using both techniques, the complex appears as an elongated particle, with a maximum dimension of 150 Å, corresponding to juxtaposition of the two partners along their longer axis. Although pb5 can be clearly recognized within the complex in the EM projection, it is not possible to fit the isolated proteins into the FhuA-pb5 SANS envelope at this resolution without further restraints. In agreement with our data, pb5 was recently unambiguously localized by immunolocalization at the tip of the straight fiber, and EM images show a similar structure of pb5 whether isolated, bound to FhuA (Fig. 5), or within the phage.[5] The comparison of EM images further suggests that monomeric pb5 has its long axis parallel to the straight fiber and that one extremity binds to the straight fiber protein, whereas the interaction with FhuA occurs via the other extremity.

Although this is the event that commits the phage to infection, little is known about the irreversible interaction between phage RBPs and their receptors at the surface of the host and subsequent signaling for cell wall puncturing and DNA ejection. An increasing number of structures of *caudovirales* RBPs (also named tail spikes) that bind cell wall polysaccharides and that are present in multicopy within the phage are now available (for a review, see Ref. 40). A more complete picture of the molecular mechanisms that signal binding to the rest of the phage comes from the resolution of larger baseplate assemblies. The structures of these host recognition apparatus are available for the *Myoviridae* coliphage T4 (41) and the *Siphoviridae* lactococcal phage p2 (42) and TP901.1 (43) at high resolution and for the *Bacillus* siphophage SPP1 at lower resolution (44, 45). T4 and p2 baseplates, whose structure has been solved before and after DNA ejection, experience large conformational changes after irreversible binding of the phage to the host, resulting from low affinity but multiple attachments of receptor binding domains (18 copies in p2) to polysaccharides. For TP901-1, the irreversible and "avid" binding mediated by 54 flexible RBPs is thought to induce minor mechanical deformations or reorientations of the baseplate components. These large or minor conformational changes within the baseplate will trigger DNA ejection. Other structural information comes from the study of the short-tailed *Podoviridae* ε15 (46), BPP-1 (47), and P-SSP7 (48). It is worth noting that for all of these phages, the structures of the isolated RBPs, when available, fit into the density of the low resolution phage structures, indicating that these proteins have an autonomous fold, irrespective of whether they are isolated or integrated in the phage structure.

---

[5] Y. Zivanovic, L. Confalonieri, L. Ponchon, R. Lurz, M. Chami, A. Flayhan, M. Renouard, A. Huet, P. Decottignies, A. R. Davidson, C. Breyton, and P. Boulanger, submitted for publication.

This is also what we observe for pb5. However, T5 differs from the phages for which structural data are available. It does not have a baseplate with multiple copies of the RBP but bears a single copy of pb5 that is located at the distal end of a central straight fiber. This RBP folds as a unique domain and binds with extremely high affinity a protein receptor (8, 10, 49).

T5 shares some structural features of its tail tip with the other well described siphophages λ and SPP1, which bear a central spike-like fiber formed by a trimer of the proteins gpJ and gp21, respectively. gpJ binds the *E. coli* porin LambB (50), and gp21 binds the *Bacillus subtilis* protein YueB (44, 45, 51), and in both cases, it is the C-terminal part of the protein that forms the RBP. In all three phages, the host recognition and binding strategy is different from phages bearing a baseplate whose structure is known. Their sophisticated adsorption mechanism relies on two types of receptors: low affinity receptors for saccharides of the LPS (T5), techtoic acids (SPP1), or the porin OmpC (λ) (52) that accelerate adsorption, and high affinity RBP, present in low copy number, that binds a protein receptor. As for T5, the mere interaction of λ (53) and SPP1 (51) with their respective receptor is enough to trigger DNA ejection. The structures of the SPP1 tail before and after DNA release show very nicely how the conformational switch is propagated as a domino-like cascade along the tail. At the level of the spike, gp21N-ter opens to allow DNA transit out of the tail. The rest of the spike is not visible on EM pictures, probably due to the disordering of the receptor binding domain (54). In the case of T5, tomography of *empty* phages bound to FhuA-containing liposomes indicates a change in the geometry of the straight fiber, which perforates the liposome membrane (38). In the unbound phage, the straight fiber and its tip appear flexible,[5] possibly to optimize the interaction with the host. Transmission of the binding information to the rest of the phage requires conformational changes within the single copy of pb5. Because structural rearrangements induced upon binding of pb5 to its receptor FhuA are not detected by either SANS or EM, we assume that they are of small amplitude. We have shown that upon binding to FhuA, pb5 undergoes secondary structure conformational changes (10). These changes could be sufficient to initiate the cascade of signaling events that lead to DNA release. This mechanism would be specific to siphophages that bare a straight fiber/spike and that bind a protein receptor.

REFERENCES

1. Stern, A., and Sorek, R. (2011) The phage-host arms race. Shaping the evolution of microbes. *BioEssays* **33,** 43–51
2. Soto, C. M., and Ratna, B. R. (2010) Virus hybrids as nanomaterials for biotechnology. *Curr. Opin. Biotechnol.* **21,** 426–438
3. Maura, D., and Debarbieux, L. (2011) Bacteriophages as twenty-first century antibacterial tools for food and medicine. *Appl. Microbiol. Biotechnol.* **90,** 851–859
4. Stone, R. (2002) Bacteriophage therapy. Food and agriculture. Testing grounds for phage therapy. *Science* **298,** 730
5. Cascales, E., and Cambillau, C. (2012) Structural biology of type VI secretion systems. *Philos. Trans. R. Soc. Lond. B Biol. Sci.* **367,** 1102–1111
6. Heller, K. J., and Bryniok, D. (1984) O antigen-dependent mutant of bacteriophage T5. *J. Virol.* **49,** 20–25
7. Boulanger, P., le Maire, M., Bonhivers, M., Dubois, S., Desmadril, M., and Letellier, L. (1996) Purification and structural and functional characterization of FhuA, a transporter of the *Escherichia coli* outer membrane. *Biochemistry* **35,** 14216–14224
8. Plançon, L., Janmot, C., le Maire, M., Desmadril, M., Bonhivers, M., Letellier, L., and Boulanger, P. (2002) Characterization of a high-affinity complex between the bacterial outer membrane protein FhuA and the phage T5 protein pb5. *J. Mol. Biol.* **318,** 557–569
9. Braun, V. (2009) FhuA (TonA), the career of a protein. *J. Bacteriol.* **191,** 3431–3436
10. Flayhan, A., Wien, F., Paternostre, M., Boulanger, P., and Breyton, C. (2012) New insights into pb5, the receptor binding protein of bacteriophage T5, and its interaction with its *Escherichia coli* receptor FhuA. *Biochimie* **94,** 1982–1989
11. Breyton, C., Gabel, F., Lethier, M., Flayhan, A., Durand, G., Jault, J.-M., Juillan-Binard, C., Imbert, L., Moulin, M., Ravaud, S., Härtlein, M., and Ebel, C. (2013) Small angle neutron scattering for the study of solubilised membrane proteins. *Eur. Phys. J. E Soft Matter* **36,** 71
12. Jacrot, B. (1976) The study of biological structures by neutron scattering from solution. *Rep. Prog. Phys.* **39,** 911
13. Timmins, P. A., and Zaccai, G. (1988) Low resolution structures of biological complexes studied by neutron scattering. *Eur. Biophys. J.* **15,** 257–268
14. Blesneac, I., Ravaud, S., Juillan-Binard, C., Barret, L.-A., Zoonens, M., Polidori, A., Miroux, B., Pucci, B., and Pebay-Peyroula, E. (2012) Production of UCP1 a membrane protein from the inner mitochondrial membrane using the cell free expression system in the presence of a fluorinated surfactant. *Biochim. Biophys. Acta* **1818,** 798–805
15. Breyton, C., Pucci, B., and Popot, J.-L. (2010) Amphipols and fluorinated surfactants. Two alternatives to detergents for studying membrane proteins *in vitro. Methods Mol. Biol.* **601,** 219–245
16. Cho, K. H., Byrne, B., and Chae, P. S. (2013) Hemifluorinated maltose-neopentyl glycol (HF-MNG) amphiphiles for membrane protein stabilisation. *Chembiochem* **14,** 452–455
17. Nehmé, R., Joubert, O., Bidet, M., Lacombe, B., Polidori, A., Pucci, B., and Mus-Veteau, I. (2010) Stability study of the human G-protein coupled receptor, Smoothened. *Biochim. Biophys. Acta* **1798,** 1100–1110
18. Talbot, J.-C., Dautant, A., Polidori, A., Pucci, B., Cohen-Bouhacina, T., Maali, A., Salin, B., Brèthes, D., Velours, J., and Giraud, M.-F. (2009) Hydrogenated and fluorinated surfactants derived from tris(hydroxymethyl)-acrylamidomethane allow the purification of a highly active yeast F1-F0 ATP-synthase with an enhanced stability. *J. Bioenerg. Biomembr.* **41,** 349–360
19. Abla, M., Durand, G., and Pucci, B. (2008) Glucose-based surfactants with hydrogenated, fluorinated, or hemifluorinated tails. Synthesis and comparative physical-chemical characterization. *J. Org. Chem.* **73,** 8142–8153
20. Breyton, C., Gabel, F., Abla, M., Pierre, Y., Lebaupain, F., Durand, G., Popot, J.-L., Ebel, C., and Pucci, B. (2009) Micellar and biochemical properties of (hemi)fluorinated surfactants are controlled by the size of the polar head. *Biophys. J.* **97,** 1077–1086
21. Abla, M., Durand, G., Breyton, C., Raynal, S., Ebel, C., and Pucci, B. (2012) A diglucosylated fluorinated surfactant to handle integral membrane proteins in aqueous solution. *J. Fluor. Chem.* **134,** 63–71
22. Ferguson, A. D., Breed, J., Diederichs, K., Welte, W., and Coulton, J. W.

(1998) An internal affinity-tag for purification and crystallization of the siderophore receptor FhuA, integral outer membrane protein from *Escherichia coli* K-12. *Protein Sci.* **7,** 1636–1638

23. Ebel, C. (2011) Sedimentation velocity to characterize surfactants and solubilized membrane proteins. *Methods* **54,** 56–66

24. Salvay, A. G., Santamaria, M., le Maire, M., and Ebel, C. (2007) Analytical ultracentrifugation sedimentation velocity for the characterization of detergent-solubilized membrane proteins Ca²⁺-ATPase and ExbB. *J. Biol. Phys.* **33,** 399–419

25. Ghosh, R., Egelhaalf, S., and Rennie, A. (2006) *A Computing Guide for Small-angle Scattering Experiments*, pp.35–100, Institute Laue-Langevin, Grenoble

26. Konarev, P. V., Volkov, V. V., Sokolova, A. V., Koch, M. H. J., and Svergun, D. I. (2003) PRIMUS. A Windows PC-based system for small-angle scattering data analysis. *J. Appl. Crystallogr.* **36,** 1277–1282

27. Jacrot, B., and Zaccai, G. (1981) Determination of molecular weight by neutron scattering. *Biopolymers* **20,** 2413–2426

28. Franke, D., and Svergun, D. I. (2009) DAMMIF, a program for rapid *ab-initio* shape determination in small-angle scattering. *J. Appl. Crystallogr.* **42,** 342–346

29. Svergun, D. I. (1992) Determination of the regularization parameter in indirect-transform methods using perceptual criteria. *J. Appl. Crystallogr.* **25,** 495–503

30. Volkov, V. V., and Svergun, D. I. (2003) Uniqueness of *ab initio* shape determination in small-angle scattering. *J. Appl. Crystallogr.* **36,** 860–864

31. Svergun, D. I., Richard, S., Koch, M. H., Sayers, Z., Kuprin, S., and Zaccai, G. (1998) Protein hydration in solution. Experimental observation by x-ray and neutron scattering. *Proc. Natl. Acad. Sci. U.S.A.* **95,** 2267–2272

32. Ludtke, S. J., Baldwin, P. R., and Chiu, W. (1999) EMAN. Semiautomated software for high-resolution single-particle reconstructions. *J. Struct. Biol.* **128,** 82–97

33. Mertens, H. D., and Svergun, D. I. (2010) Structural characterization of proteins and complexes using small-angle x-ray solution scattering. *J. Struct. Biol.* **172,** 128–141

34. Compton, E. L., Karinou, E., Naismith, J. H., Gabel, F., and Javelle, A. (2011) Low resolution structure of a bacterial SLC26 transporter reveals dimeric stoichiometry and mobile intracellular domains. *J. Biol. Chem.* **286,** 27058–27067

35. Clifton, L. A., Johnson, C. L., Solovyova, A. S., Callow, P., Weiss, K. L., Ridley, H., Le Brun, A. P., Kinane, C. J., Webster, J. R., Holt, S. A., and Lakey, J. H. (2012) Low resolution structure and dynamics of a colicin-receptor complex determined by neutron scattering. *J. Biol. Chem.* **287,** 337–346

36. Rambo, R. P., and Tainer, J. A. (2013) Super-resolution in solution X-ray scattering and its applications to structural systems biology. *Annu. Rev. Biophys.* **42,** 415–441

37. Udho, E., Jakes, K. S., and Finkelstein, A. (2012) TonB-dependent transporter FhuA in planar lipid bilayers. Partial exit of its plug from the barrel. *Biochemistry* **51,** 6753–6759

38. Böhm, J., Lambert, O., Frangakis, A. S., Letellier, L., Baumeister, W., and Rigaud, J. L. (2001) FhuA-mediated phage genome transfer into liposomes. A cryo-electron tomography study. *Curr. Biol.* **11,** 1168–1175

39. Zoued, A., Durand, E., Bebeacua, C., Brunet, Y. R., Douzi, B., Cambillau, C., Cascales, E., and Journet, L. (2013) TssK is a trimeric cytoplasmic protein interacting with components of both phage-like and membrane anchoring complexes of the Type VI secretion system. *J. Biol.*

Chem. **288,** 27031–27041

40. Veesler, D., and Cambillau, C. (2011) A common evolutionary origin for tailed-bacteriophage functional modules and bacterial machineries. *Microbiol. Mol. Biol. Rev.* **75,** 423–433

41. Leiman, P. G., Arisaka, F., van Raaij, M. J., Kostyuchenko, V. A., Aksyuk, A. A., Kanamaru, S., and Rossmann, M. G. (2010) Morphogenesis of the T4 tail and tail fibers. *Virol. J.* **7,** 355

42. Sciara, G., Bebeacua, C., Bron, P., Tremblay, D., Ortiz-Lombardia, M., Lichière, J., van Heel, M., Campanacci, V., Moineau, S., and Cambillau, C. (2010) Structure of lactococcal phage p2 baseplate and its mechanism of activation. *Proc. Natl. Acad. Sci. U.S.A.* **107,** 6852–6857

43. Veesler, D., Spinelli, S., Mahony, J., Lichière, J., Blangy, S., Bricogne, G., Legrand, P., Ortiz-Lombardia, M., Campanacci, V., van Sinderen, D., and Cambillau, C. (2012) Structure of the phage TP901-1 1.8 MDa baseplate suggests an alternative host adhesion mechanism. *Proc. Natl. Acad. Sci. U.S.A.* **109,** 8954–8958

44. Goulet, A., Lai-Kee-Him, J., Veesler, D., Auzat, I., Robin, G., Shepherd, D. A., Ashcroft, A. E., Richard, E., Lichière, J., Tavares, P., Cambillau, C., and Bron, P. (2011) The opening of the SPP1 bacteriophage tail, a prevalent mechanism in Gram-positive-infecting siphophages. *J. Biol. Chem.* **286,** 25397–25405

45. Vinga, I., Baptista, C., Auzat, I., Petipas, I., Lurz, R., Tavares, P., Santos, M. A., and São-José, C. (2012) Role of bacteriophage SPP1 tail spike protein gp21 on host cell receptor binding and trigger of phage DNA ejection. *Mol. Microbiol.* **83,** 289–303

46. Chang, J. T., Schmid, M. F., Haase-Pettingell, C., Weigele, P. R., King, J. A., and Chiu, W. (2010) Visualizing the structural changes of bacteriophage ε15 and its *Salmonella* host during infection. *J. Mol. Biol.* **402,** 731–740

47. Dai, W., Hodes, A., Hui, W. H., Gingery, M., Miller, J. F., and Zhou, Z. H. (2010) Three-dimensional structure of tropism-switching *Bordetella* bacteriophage. *Proc. Natl. Acad. Sci. U.S.A.* **107,** 4347–4352

48. Liu, X., Zhang, Q., Murata, K., Baker, M. L., Sullivan, M. B., Fu, C., Dougherty, M. T., Schmid, M. F., Osburne, M. S., Chisholm, S. W., and Chiu, W. (2010) Structural changes in a marine podovirus associated with release of its genome into Prochlorococcus. *Nat. Struct. Mol. Biol.* **17,** 830–836

49. Basit, H., Sharma, K. S., Van der Heyden, A., Gondran, C., Breyton, C., Dumy, P., Winnik, F. M., and Labbé, P. (2012) Amphipol mediated surface immobilization of FhuA. A platform for label-free detection of the bacteriophage protein pb5. *Chem. Commun. (Camb.)* **48,** 6037–6039

50. Wang, J., Hofnung, M., and Charbit, A. (2000) The C-terminal portion of the tail fiber protein of bacteriophage λ is responsible for binding to LamB, its receptor at the surface of *Escherichia coli* K-12. *J. Bacteriol.* **182,** 508–512

51. São-José, C., Lhuillier, S., Lurz, R., Melki, R., Lepault, J., Santos, M. A., and Tavares, P. (2006) The ectodomain of the viral receptor YueB forms a fiber that triggers ejection of bacteriophage SPP1 DNA. *J. Biol. Chem.* **281,** 11464–11470

52. Montag, D., Schwarz, H., and Henning, U. (1989) A component of the side tail fiber of *Escherichia coli* bacteriophage λ can functionally replace the receptor-recognizing part of a long tail fiber protein of the unrelated bacteriophage T4. *J. Bacteriol.* **171,** 4378–4384

53. Roessner, C. A., Struck, D. K., and Ihler, G. M. (1983) Injection of DNA into liposomes by bacteriophage λ. *J. Biol. Chem.* **258,** 643–648

54. Plisson, C., White, H. E., Auzat, I., Zafarani, A., São-José, C., Lhuillier, S., Tavares, P., and Orlova, E. V. (2007) Structure of bacteriophage SPP1 tail reveals trigger for DNA ejection. *EMBO J.* **26,** 3720–3728